Nanoelectrode Scanning Probes from Fluorocarbon-Coated Single-Walled Carbon Nanotubes

ARTICLE *in* NANO LETTERS · AUGUST 2004

Impact Factor: 13.59 · DOI: 10.1021/nl048991s

NANO LETTERS

2004
Vol. 4, No. 10
1873−1879

Nanoelectrode Scanning Probes from Fluorocarbon-Coated Single-Walled Carbon Nanotubes

Maria J. Esplandiu,† Vern G. Bittner, Konstantinos P. Giapis,* and C. Patrick Collier*

Division of Chemistry and Chemical Engineering, California Institute of Technology, Pasadena, California 91125

Received June 29, 2004; Revised Manuscript Received July 29, 2004

ABSTRACT

We have developed a method to coat single-walled carbon nanotubes attached to AFM tips with conformal fluorocarbon polymer films formed in an inductively coupled plasma reactor. The polymer provides a chemically inert and electrically insulating outer layer and mechanically stabilizes the attached nanotube sufficiently to enable imaging in liquids without the need for an intervening adhesive. Electrical pulse etching of the insulating coating exclusively at the nanotube tip end results in well-defined highly conductive nanoelectrodes. For these probes, the conductive properties of the nanotubes are not affected by the coating. Some nanoelectrodes behave as rectifying diodes, which may be developed into novel molecular devices integrated onto scanning probes.

When attached to conventional atomic force microscope (AFM) tips, carbon nanotubes can be used for ultrahigh-resolution imaging and manipulation at the nanoscale.[1−10] Chemical and biological functionalization of nanotube tips[3,10] and the construction of conducting nanotube probes[8,11−12] have expanded the capabilities of these tools beyond topographical imaging applications. Of particular interest is the fabrication of functionalized "nanoelectrodes" integrated on scanning probes for point-source sensing or triggering of local bioelectrochemical reactions in aqueous physiologically relevant environments.

To maximize the utility of such nanoelectrode scanning probes, the electrochemical activity must be limited to the nanotube tip end. This requires passivation and electrical insulation of the nanotube, AFM tip support, and cantilever assembly except for the selective removal of the insulator at the nanotube tip end. Crooks et al.[13] first reported fabrication and characterization of nanoelectrodes from individual 100 nm diameter multiwalled carbon nanotubes (MWNTs). The MWNTs were coated with an insulating layer formed by electrochemical polymerization reactions of polyphenol. Removal of the coating from the nanotube tip end was accomplished by electrochemical etching or by electrical pulse etching in air. However, consistent etching of the insulating coating without destruction of the nanotube itself was difficult to achieve.[14] Recently, Rinzler et al.[15] described a method for coating long (2−3 μm) MWNT probes in the vapor phase based on high-temperature Parylene polymerization followed by laser-induced vaporization of the coating at the nanotube end.

In this paper, we describe a new method for coating single-walled carbon nanotube (SWNT) probes attached to AFM tips. Ultimate resolution and precision in imaging and manipulation applications can be accomplished only with *individual* SWNTs. However, such probes generally suffer from buckling and bending instabilities that can limit their utility. We use room temperature plasma-assisted decomposition of fluorocarbon gases to deposit Teflon-like polymer coatings of controlled composition and thickness on the nanotubes. In addition to superb chemical inertness and insulating properties, the fluorocarbon polymer reinforces the attachment of the nanotube to the AFM tip without the use of adhesives. Further, these coatings significantly enhance the rigidity of single-walled nanotube probes, increasing their usefulness and functionality. Finally, electrical pulse etching of the coated nanotube probe exposes its tip end, resulting in a nanoelectrode that can be further functionalized.

With this procedure, we have constructed nanoelectrode probes consisting of both metallic and semiconducting SWNTs attached to gold-coated AFM tips and have characterized their electrical properties by contacting them to a liquid mercury (Hg) droplet, following methodology described in the literature.[11,16] For these nanoelectrodes, the electrical properties of the SWNTs were not changed by the coating. For some probes, we observed strongly rectifying

* Corresponding authors. E-mail: collier@caltech.edu, giapis@cheme.caltech.edu.
† Current address: Departament de Quimica, Universitat Autonoma de Barcelona.

10.1021/nl048991s CCC: $27.50
Published on Web 08/19/2004

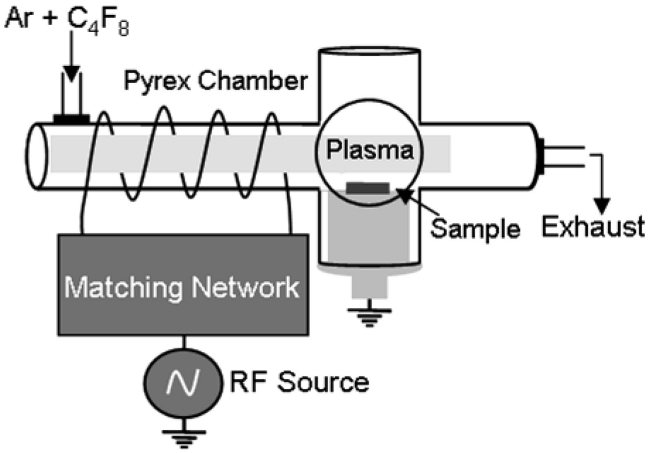

Figure 1. Schematic of the inductively coupled plasma reactor.

behavior in the $I-V$ curves at positive potentials, reminiscent of previously reported metal−semiconductor heterojunctions in single-walled carbon nanotubes.[17] We have also fabricated for the first time semiconducting nanoelectrodes consisting of individual SWNTs attached to n-type silicon AFM tips without a gold precoating. The conductive properties of these nanoelectrodes were dominated by the n-type silicon.

A Digital Instruments (Santa Barbara, CA) Multimode atomic force microscope with a Nanoscope IV controller was used for this work. Transmission electron microscopy (TEM) images were taken with a Phillips EM430 microscope operating at 300 kV. The growth of single-walled carbon nanotubes by chemical vapor deposition has been described previously.[9] As-grown SWNTs were mounted on either bare silicon AFM tips (FESP, NanoWorld) or gold-coated tips (evaporation of 10 nm Cr followed by 50 nm Au) using the pick-up technique developed by Lieber and co-workers.[4] The length of the protruding nanotubes was variable, ranging from 40 to 350 nm, with an average diameter of 5 nm. The maximum *total* length of our SWNT probes is roughly equivalent to the length of just the exposed regions of the Parylene-coated MWNT probes described by Rinzler et al.[15]

Fluorocarbon deposition was performed in an inductively coupled plasma (ICP) reactor, specifically designed for coating these tips. We developed a unique plasma deposition process that virtually eliminates ion bombardment of the probes, which is damaging to the carbon nanotubes. This required careful optimization of several key operating parameters, such as the type and relative composition of gases used, flow rates, pressure, rf power, and deposition time. The end result is a process that generates a variety of precursor species under mild conditions that do not chemically react with the nanotube or the AFM tip support, but nevertheless polymerize readily on the probe, forming a compact uniform coating.

The reactor assembly, schematically shown in Figure 1, consists of a six-way Pyrex glass chamber (i.d. = 100 mm) with an upstream extension tube to accommodate a 4-turn copper tube antenna. Power was supplied to the antenna from a 600 W variable radio frequency amplifier driven by a sinusoidal waveform at 21 MHz. A conventional π-network matchbox was used to ensure precise impedance matching. The reactor was supplied with argon and octafluorocyclobutane (C_4F_8), premixed with separate mass flow controllers at the desired flow rates. Typical conditions for the conformal coating of the tip assemblies were as follows: 7 sccm Ar, 1.2 sccm C_4F_8, reactor pressure = 160 mTorr, rf power = 50−75 W for 60 to 90 s. Multiple probes were assembled on a doped Si wafer with the nanotubes pointing up, and the wafer was in electrical contact with an aluminum electrode positioned downstream from the plasma generation region. This electrode was connected externally to the network matchbox ground.

Fluorocarbon layers were also deposited on flat surfaces of silicon (100), polycrystalline Au, and highly oriented pyrolytic graphite (HOPG) for surface analysis and electrochemical studies. The silicon and Au surfaces were model surfaces for the AFM tips used while the HOPG surfaces were taken as an approximation to the carbon nanotubes. Film morphology, composition, thickness, and electrical and mechanical properties were evaluated by a number of different techniques: AFM, TEM, ellipsometry, XPS (X-ray photoelectron spectroscopy), and electrochemical impedance spectroscopy. Experimental details and data from these studies are included in the Supporting Information.

Film thicknesses determined by XPS and ellipsometry gave mutually consistent results. AFM measurements of coated HOPG substrates indicated that the film growth was highly conformal, reproducing the underlying step-terrace topography of freshly cleaved graphite. For thin polymer films (thickness less than 30 nm) the root-mean-squared surface roughness values on silicon, gold, and HOPG did not change from those of the uncoated surfaces, while for thicker films, the surface roughness of the coating increased slightly. XPS measurements showed that the composition of the film could be controlled by fine-tuning the plasma operation. The plasma operating conditions were adjusted so that the CF_2 component had the highest intensity in the XPS spectra, consistent with a more Teflon-like polymer.

Electrochemical impedance spectroscopy gave 8.5×10^{11} Ω·m for the resistivity and 2.3 for the dielectric constant of these films. The dielectric constant falls within the range reported for fluorocarbon polymers (2.1−2.6). Although the thin-film resistivity was lower than the bulk resistivity reported for bulk Teflon ($\sim 10^{16}$ Ω·m),[18] it is important to note that these films were less than 30 nm thick. TEM images showed that the fluorocarbon coatings were deposited uniformly and conformally on nanotube AFM tips.

The coatings significantly enhance the mechanical stability of SWNT probes, as observed by Rinzler and co-workers for MWNTs.[15] We have used coated SWNT tips that are hundreds of nm long to image prone SWNTs on the growth substrate in tapping mode (see Supporting Information). The lateral resolution of the images (full width minus height) was equal to the width of the probe as measured by TEM. Imaging with uncoated SWNT probes having these lengths would be virtually impossible due to their lateral flexibility, which leads to severe artifacts from buckling and bending instabilities.[9,19]

The electrical insulating properties of the polymer coatings were characterized using tapping mode AFM as the probe came into contact with a small (less than 200 μm) drop of liquid mercury. The procedure we used is similar to that reported by Wilson, et al. for measuring the conductive properties of uncoated SWNT tips,[11] except in our case, we measured the conductive properties of the coated nanotube probe both before and after the probe end had been exposed by electrical pulse etching. The liquid Hg drop used in this work served multiple purposes. First, it provided a conductive surface for etching away the fluorocarbon polymer from the probe when electrical pulses were applied to the tip. Second, it provided excellent electrical contact with the probe at all immersion depths, which allowed for a thorough assessment of the insulating coatings. By comparing the conductive properties of the probe as a function of immersion depth, both before and after electrical pulse etching, we unequivocally determined that the etching was localized at the nanotube tip end.

The AFM was shielded using a Faraday cage. The coated nanotube probe was placed in an electrostatic force microscopy (EFM) tip holder, which allowed the direct application of potentials to the tip in combination with a Digital Instruments Signal Access Module. A computer data acquisition card was used to generate steady-state voltages for monitoring the tip conductivity and generating current−voltage ($I-V$) curves. The current from the mercury contact was measured at virtual ground and converted to voltage by a current preamplifier (Keithley 486 picoammeter). For electrical pulse etching, an HP 8114A pulse generator was used.

The nanotube tip was first engaged in tapping mode on the surface of the Hg droplet. The AFM controller was then immediately switched to tapping mode force calibration, which consists of monitoring the cantilever oscillation amplitude and deflection as functions of the *z*-piezo displacement (cycled continuously at 1 Hz). This permits simultaneous monitoring of the conductivity, the immersion depth, and the length and integrity of the nanotube probe. For uncoated SWNT probes, the nanotube bends or buckles elastically at higher loads and does not deflect the cantilever. The distance between the point at which the oscillation amplitude decreases to zero and the point at which the deflection of the cantilever is detected indicates the protrusion length of the nanotube. For SWNT probes coated with the polymer, the amplitude and deflection signals are modified slightly due to the increased rigidity of the coated nanotube. The coated nanotube can now deflect the cantilever as it makes contact with the surface, but to a lesser extent than the more rigid AFM tip. Thus, there is a change in the slope of the deflection signal when the silicon tip makes contact with the surface. The damping of the oscillation amplitude relative to the changes in the deflection signal of the probe as it comes into contact with the mercury drop allowed us to discriminate between the regions where only the coated nanotube is immersed in the mercury from where the larger more rigid silicon or gold-coated silicon tip contacts the liquid.

Two types of measurements were performed. For a fixed potential applied to the tip, the current and probe deflection were monitored as the tip was immersed into the Hg drop. Simultaneous measurement of the current and tip deflection was accomplished as a function of the immersion depth by feeding the preamplifier output back into the Nanoscope IV controller.

Alternatively, at fixed *z*-displacement, current−potential ($I-V$) curves were recorded, either in the region where only the nanotube was immersed, or where the entire probe assembly (nanotube and AFM pyramidal tip support) was immersed in the Hg droplet. The immersion depth was kept constant (for long enough times to capture $I-V$ curves) by fixing the *z*-scan start value of the piezo and by imposing a zero value for the scan ramp size. $I-V$ curves were generated from 10 to 20 mV steps at scan rates of 200−300 steps per second.

The electrical conductivity of the fluorocarbon polymer coated nanotube probe was first measured as a function of immersion depth in liquid Hg in order to test the insulating properties of the polymer. This is shown in Figure 2 for a probe consisting of a 100 nm long insulated nanotube attached to a gold coated silicon probe. $I-V$ curves were captured at two different immersion depths as indicated by regions A and B in the amplitude and deflection versus *z*-displacement traces. Region A corresponds to the deflection of the coated nanotube only, while region B, defined by the change in slope of the deflection signal, corresponds to physical contact of the AFM tip support with the Hg.

Due to the highly insulating coating, no current was recorded above the detection limit of our picoammeter at any immersion depth for potentials ranging from −1.5 V to 1.5 V, Figure 2c. However, after etching with a 5 V, 10 μs electrical pulse, large currents flowed through the nanotube to the Hg contact, Figure 2d. The $I-V$ curve is symmetric with a low-bias resistance of 177 kΩ, which is within the range of values reported for the lowest measured contact resistances between (uncoated) metallic SWNTs and gold-coated AFM tips[11] or lithographically defined gold electrodes.[20]

This behavior indicates that coating the probe with the fluorocarbon polymer did not change the electrical conductivity of the metallic nanotube, nor did it affect the contact resistance between it and the gold-coated AFM tip. It is also important to note that no significant change in the current was detected between curves A and B, either before or after the polymer was etched, which demonstrates unambiguously that the insulating polymer coating was preserved intact except at the very end of the nanotube.

This conclusion is strengthened further by the simultaneous measurement of the probe deflection and current from another metallic nanotube as it made repeated contact with the Hg drop. Figure 3 shows both the trace (immersion) and retrace (withdrawal) of an 80 nm long coated nanotube probe attached to a gold-coated AFM tip that had been previously etched by an electrical pulse. The curves were recorded at a fixed tip potential of −0.5 V. The deflection retrace curve shown in Figure 3 reveals the breaking of a meniscus neck

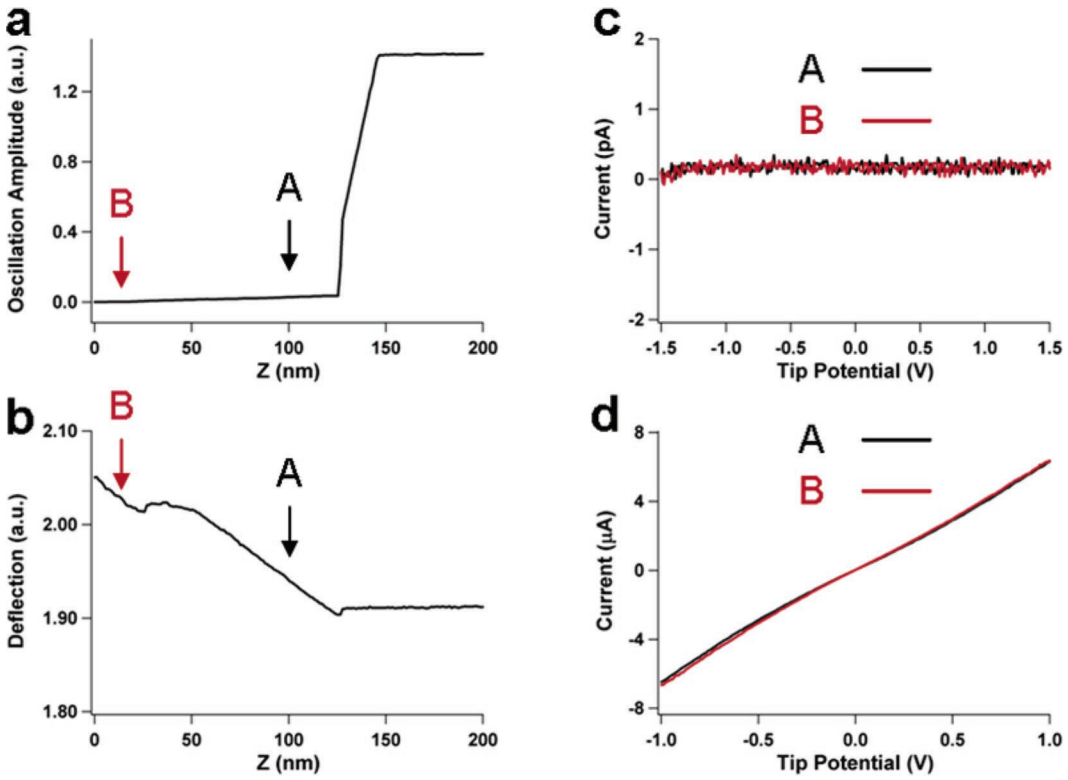

Figure 2. (a) Oscillation amplitude and (b) deflection vs *z*-displacement for a nanoelectrode probe consisting of a metallic nanotube attached to a gold-coated AFM tip in contact with a mercury droplet (before applying an electrical etch pulse). (c,d) $I-V$ curves taken at the immersion depths indicated with arrows A and B. (c) was recorded before and (d) was recorded after applying a 5 V electrical etching pulse for 10 μs to the probe.

at the nanotube tip end as the probe was being withdrawn from the liquid Hg surface. This position corresponds exactly to the loss of current from the tip. Assuming Hg does not wet the hydrophobic fluorocarbon polymer coating or the exposed nanotube,[21] the region of physical contact with the probe at this position will be limited to the last few nanometers of the probe. This represents additional evidence that the conductivity was measured only from the exposed nanotube tip end.

The disruptions in the retrace deflection curves provide valuable information, because they correspond uniquely to the point where both physical and electrical contact between the probe and the Hg was lost and thus can be correlated with current versus position curves. The trace curves, on the other hand, cannot provide as much information due to uncertainties in nanotube position from bending or buckling instabilities of the coated nanotube as it attempts to penetrate the high energy Hg surface (500 mJ/m^2).

There was initially no current when the probe first makes contact with and pushes against the Hg drop surface. The current was only detected after the probe had been retracted from its lowest position by about 5 nm. We believe that at first contact the coated nanotube tended to bend on the Hg surface but did not penetrate due to the high surface tension of the drop. The nanotube tip needed to be pushed harder against the Hg surface in order to penetrate it and give a measurable current. Similar effects had been reported previously for multiwalled carbon nanotubes contacted to Hg drops in situ in a TEM.[22] Precisely when this occurs as a function of *z*-displacement will vary randomly from one case to the next (see Supporting Information), but it will be very dependent on the nanotube orientation with respect to the surface normal and its length. For shorter and more vertically oriented nanotubes, bending or buckling effects are minimized and we expect this would correlate to the ability of the nanotube probe to reproducibly penetrate the mercury droplet.

Figure 4 is a subsequent TEM image of the same probe used to generate the data in Figure 2. The image shows that, as a consequence of the pulse, the probe had been shortened to 80 nm, which matches the length determined from amplitude and deflection curves taken for this probe after pulse etching (data not shown). The fact that these data were taken after the conductivity experiments indicates that these probes are very robust and can survive multiple experimental procedures under very different conditions and at different locations. The diameter of the nanotube probe was 15 nm, which would correspond to ~5 nm polymer coating thickness, assuming the diameter of this SWNT was equal to the average value of 5 nm. Coating thicknesses in the range 5−10 nm were consistently obtained using the plasma conditions employed here.

Apparently the electrical pulse sharply cut the coated nanotube without significant removal of the polymer coating the sidewalls of the nanotube above the etched point. Close inspection of the TEM image (inset) shows structure at the probe apex that may be a signature of etching of the polymer coating to expose the nanotube tip end, although the lack of

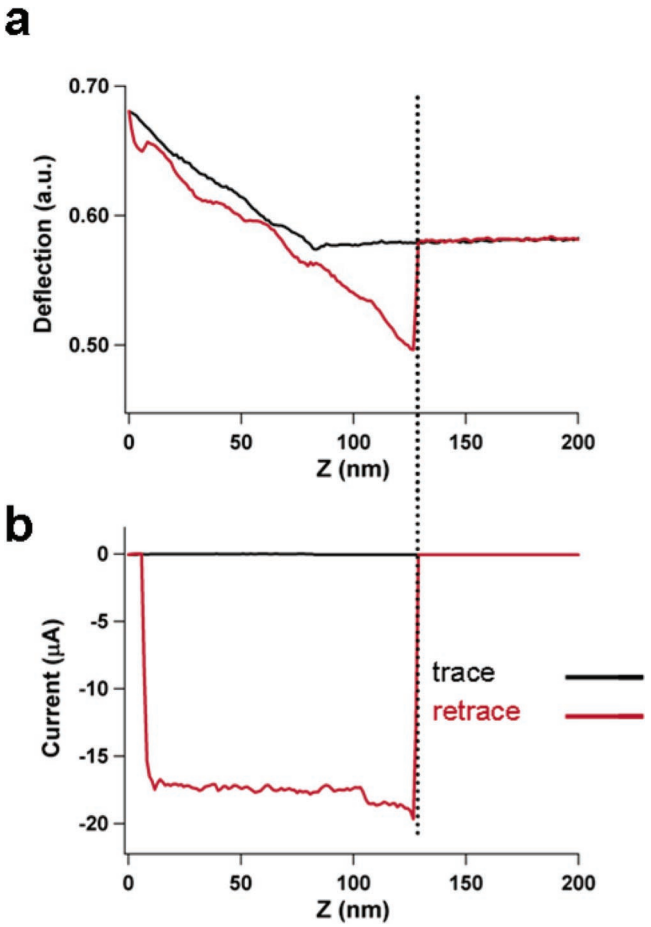

Figure 3. Deflection and current profiles of the probe as it was penetrating and retracting from the Hg drop. The tip was held at a potential of −0.5 V.

contrast between the fluorocarbon polymer and the nanotube in the image renders visual confirmation of tip exposure difficult. It is also plausible that local heating by the electron beam in the TEM caused some healing of the etched site. Local morphological changes of bare SWNTs due to heating effects in TEM have been reported previously.[23]

The transport characteristics of the two highly conductive metallic nanoelectrodes described above were stable during repeated cycling of the probes in the Hg drop, which suggests that these nanotubes had an optimal orientation relative to the drop surface. In many cases, gradual mechanical degradation of nanotube probes occurred as a result of repeated penetration into the high energy surface of the drop, even for coated tubes. We expect that this would not be as much of a problem for a probe that is continuously immersed in an aqueous environment. Degradation or etching of highly conductive nanotube probes can also occur at steady-state (not pulsed) tip potentials above one volt, due to the high current densities that flow through the SWNTs ($>10^7$ A/cm^2). This effect was also seen with MWNTs contacted to Hg.[22]

In addition to highly conductive nanoelectrode probes assembled from metallic SWNTs on gold tips, we have also observed three very different modes of semiconducting behavior from nanoelectrodes as shown in Figure 5. Figure 5a is an $I-V$ curve from a 250 nm long semiconducting

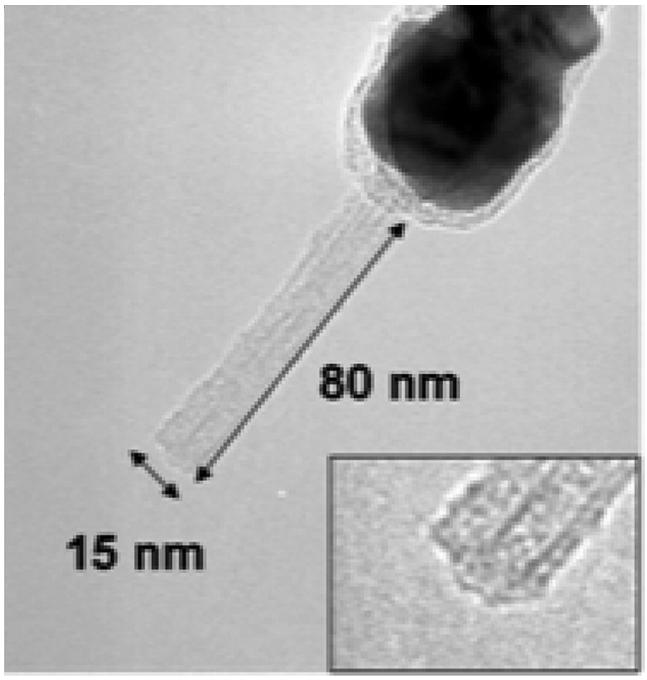

Figure 4. TEM image of the etched nanotube probe used in Figure 2. The nanotube was shortened to 80 nm after applying a 5 V electrical pulse.

nanotube contacted to a gold AFM tip. As before, no current was recorded from the insulated probe either as a function of the immersion depth or as a function of the voltage. After applying a 5 V etching pulse, the nanotube was shortened to 135 nm and the resulting $I-V$ curve exhibited nonlinear and slightly asymmetric conductivity with a high resistance at low-bias (850 MΩ), similar to the uncoated semiconducting nanotube described by Wilson and co-workers.[11]

The $I-V$ curves in Figure 5b and 5c are highly asymmetric and actually resemble the conductive properties of rectifying diodes. The $I-V$ curve in Figure 5b was from a probe fabricated using a silicon AFM tip support that was not precoated with gold and shows diode-like behavior with strong current rectification at negative bias. The limiting barrier for conduction through the probe in this case is the 1−2 nm thick native silicon oxide layer that forms between the carbon nanotube and the n-type silicon tip. There is a much smaller Schottky barrier between the nanotube and the Hg,[11] leading to the strongly asymmetric $I-V$ curves observed. A control experiment with a bare silicon AFM tip immersed in Hg (no attached nanotube and no fluorocarbon polymer) showed similar behavior, although at much higher current (see Supporting Information). This is consistent with a mercury−insulator−silicon (n-type) tunnel junction having significantly higher currents at forward bias (negative potential applied to the tip) than the saturation current at reverse bias.[24] The electronic nature of the nanotube (metallic or semiconductor) for this probe thus cannot be determined from this measurement due to the strong influence of the silicon contact, which determines the overall electrical behavior of the system.

The positive current rectification seen in Figure 5c is more difficult to rationalize. The $I-V$ curve in this case was

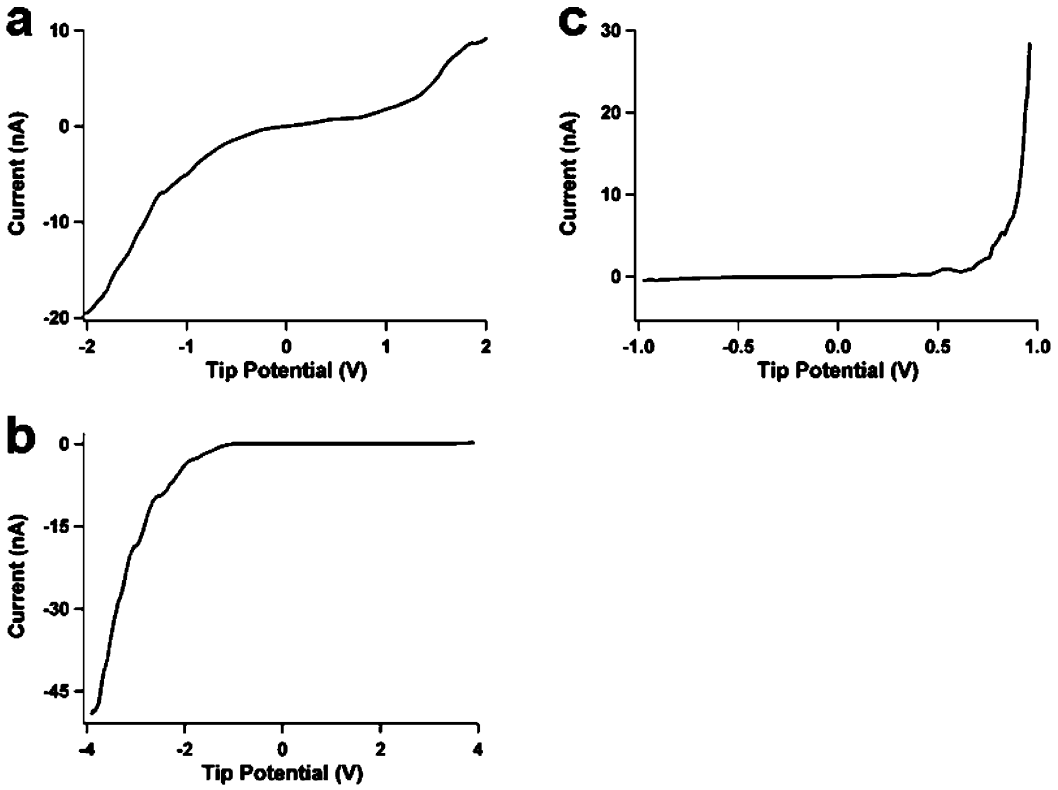

Figure 5. (a) $I-V$ curve of a probe consisting of a semiconducting nanotube electrically contacted to a gold-coated AFM tip. (b) Negative rectification in the $I-V$ characteristic of a nanoelectrode probe which had an n-type silicon tip without gold as the support for the nanotube. (c) $I-V$ curve showing positive rectification for nanotube attached to a gold-coated tip.

generated from a 180 nm long insulated nanotube attached to a gold-coated silicon probe, etched with a 5 V pulse. This behavior has been seen from three other nanotube probes as well; two of them were contacted to gold-coated AFM tips, but one was contacted to a silicon probe that was not precoated with gold (see Supporting Information). All four of these probes exhibited the same positive rectification characteristics, although the current was lower for the nanotube attached to the silicon AFM tip. The $I-V$ characteristics for these probes were stable during repeated measurements. This behavior was not seen in control experiments employing either silicon or gold-coated AFM tips where no nanotube was present.

It is known that semiconducting nanotubes are normally p-doped when contacted to metal electrodes.[25] The rectifying behavior will be determined by which contact has the lower barrier for hole injection into the nanotube. For the nanotube electrodes in Figures 5a and 5b, it is the mercury contact that has the lowest (Schottky) barrier for hole conduction, which is consistent with the current being greater at more negative tip bias. The positive rectifying behavior in Figure 5c, on the other hand, implies that the barrier for conduction is lowest at the AFM tip attachment site, even when the tip has a native oxide layer, as is the case for the silicon AFM tip.

One possibility is that this positive rectifying behavior was due to the formation of a metal-semiconductor heterojunction in the nanotube. Similar transport behavior has been observed in measurements of the $I-V$ characteristics on isolated kink junctions in SWNTs connected to lithographically defined gold electrodes on silicon by Dekker and co-workers.[17] Nanotube heterojunctions can be induced either by the formation of a pentagon−heptagon (5−7) defect pair during the growth process or by mechanical perturbations of the nanotube[17,26] The rectifying diode-like behavior for the nanotube depicted in Figure 5c was stable for multiple repeated cycling of the probe in the Hg drop, which implies that if a heterojunction was responsible for this behavior, it likely was a result of either a 5−7 defect or an irreversible mechanical deformation that occurred prior to the measurement.

However, we cannot rule out the possibility that this behavior was due to other causes, since we did not explicitly observe a heterojunction. Other issues such as poor electrical contact between the nanotube and the electrodes may be relevant, although we expect that this would affect the overall resistance values but not the nature of the strong rectification in the $I-V$ profile, which should depend more on materials properties such as work functions. Tunneling conduction between multiple nanotubes in a bundle is also a possibility, although it is remote since we have determined the operating conditions that consistently result in pick-up of only individual SWNTs.[9]

The rectifying behavior observed by Dekker et al. could be definitively assigned to a semiconductor−metal heterojunction, since it was measured across a sharp kink in the nanotube, which was imaged with AFM. We did not capture TEM images of any of the four probes that displayed this behavior. A direct correlation between a TEM image of a kinked or bent nanotube probe with the diode-like positive

rectification in the $I-V$ trace such as that shown in Figure 5c would strengthen the conclusion that a metal−semiconductor heterojunction in the nanotube was responsible.

In conclusion, we have demonstrated a new method for coating individual SWNTs attached to AFM probes with a conformal Teflon-like polymer film formed from gas-phase reactions of octofluorocyclobutane in an inductively coupled plasma reactor. The deposition was performed with the tips mounted on a grounded substrate to prevent plasma sheath formation and the concomitant ion bombardment that damages the nanotubes. Plasma parameters such as rf power, pressure, and flow rates were optimized to obtain conformal films of the desired chemical composition, thickness, and electrical properties. Nanoelectrode scanning probes were subsequently fabricated by localized electric pulse etching of the polymer at the nanotube tip end. The coatings provide superior chemical inertness and dielectric insulation. Furthermore, they reinforce the attachment site of the nanotube with the AFM tip support without the need of an adhesive, which increases the mechanical stability of the nanotube, enabling the use of longer SWNT probes. In addition to highly conductive nanoelectrodes consisting of individual metallic SWNTs contacted to gold AFM tips, we have demonstrated semiconducting probes having both positive and negative current rectification characteristics. This suggests the possibility of developing new kinds of scanning probes that can function as nanodiodes.

Acknowledgment. The authors thank Lawrence Wade, Jordan Gerton, and David Lopez for helpful discussions. We acknowledge Dr. P.-L-M. Noeske, Fraunhofer Institute, IFAM, Bremen for expertise in the measurements of XPS spectra at high resolution and at low fluorocarbon film thicknesses. We also acknowledge the help of Shannon Lewis with XPS measurements and Carol Garland with TEM imaging. This work was supported by Caltech startup funds and by Arrowhead Research.

Supporting Information Available: Fluorocarbon film thickness determination and chemical composition by ellipsometry and XPS, AFM images of film morphology, electrochemical impedance spectroscopy and cyclic voltammetry, additional deflection and current profiles from same probe used to generate Figure 3, TEM images of coated nanotube probes, AFM tapping mode image taken with coated nanotube probe, $I-V$ curves from bare silicon AFM tip and polymer-coated nanotube attached to silicon AFM tip. This material is available free of charge via the Internet at http://pubs.acs.org.

References

(1) Dai, H.; Hafner, J. H.; Rinzler, A. G.; Colbert, D. T.; Smalley, R. E. *Nature* **1996**, *284*, 147.
(2) Cheung, C.-L.; Hafner, J. H.; Odom, T. W.; Kyoungha, K.; Lieber, C. M. *Appl. Phys. Lett.* **2000**, *76*, 3136.
(3) Wong, S. S.; Wooley, A. T.; Joselevich, E.; Cheung, C.-L.; Lieber, C. M. *J. Am. Chem. Soc.* **1998**, *120*, 8557.
(4) Hafner, J. H.; Cheung, C.-L.; Oosterkamp, T. H.; Lieber, C. M. *J. Phys. Chem. B* **2001**, *105*, 743.
(5) Yenilmez, E.; Qian, W.; Chen, R. J.; Dunwei, W.; Dai, H. *Appl. Phys. Lett.* **2002**, *80*, 2225.
(6) De Jonge, N.; Lamy, Y.; Kaiser, M. *Nano Lett.* **2003**, *3*, 1621.
(7) Hafner, J. H.; Cheung, C.-L.; Lieber, C. M. *Nature* **1999**, *398*, 761.
(8) Cooper, E. B.; Manalis, S. R.; Fang, H.; Dai, H.; Minne, S. C.; Hunt, T.; Quate, C. F. *Appl. Phys. Lett.* **1999**, *75*, 3566.
(9) Wade, L. A.; Shapiro, I. R.; Ma, Z.; Quake, S. R.; Collier, C. P. *Nano Lett.* **2004**, *4*, 725.
(10) Wong, S. S.; Joselevich, E.; Woolley, A. T.; Cheung, C.-L.; Lieber, C. M. *Nature* **1998**, *394*, 52.
(11) Wilson, N. R.; Cobden, D. H.; Macpherson, J. V. *J. Phys. Chem. B* **2002**, *106*, 13102.
(12) Wilson, N. R.; Macpherson, J. V. *Nano Lett.* **2003**, *3*, 1365.
(13) Campbell, J. K.; Sun, L.; Crooks, R. M. *J. Am. Chem. Soc.* **1999**, *121*, 3779.
(14) Ito, T.; Sun, L.; Crooks, R. M. *Electrochem. Solid-State Lett.* **2003**, *6*, C4.
(15) Patil, A.; Sippel, J.; Martin, G. W.; Rinzler, A. G. *Nano Lett.* **2004**, *4*, 303.
(16) Frank, S.; Poncharal, P.; Wang, Z. L.; de Heer, W. A. *Science* **1998**, *280*, 1744.
(17) Yao, Z.; Postma, H. W. C.; Balents, L.; Dekker, C. *Nature* **1999**, *402*, 273.
(18) Dupont Teflon and Tefzel properties specification bulletin, on the web at http://www.dupont.com/Teflon/films/H-04321−2.html.
(19) Snow, E. S. Campbell, P. M. Novak, J. P. *Appl. Phys. Lett.* **2002**, *80*, 2002.
(20) Yao, Z.; Kane, C. L.; Dekker, C. *Phys. Rev. Lett.* **2000**, *84* 2941.
(21) Dujardin, E.; Ebbesen, T.; Hiura, H.; Tanigaki, K. *Science* **1994**, *265*, 1850.
(22) Berger, C.; Yi, Y.; Gezo, J.; Poncharal, P.; de Heer, W. A. *N. J. Phys.* **2003**, *5*, 158.1
(23) Kiang, C.-H.; Goddard, W. A.; Beyers, R.; Bethune, D. S. *J. Phys. Chem.* **1996**, *100*, 3749.
(24) Liu, Y.-J.; Yu, H.-Z. *ChemPhysChem* **2003**, *4*, 335.
(25) Tans, S. J.; Verschueren, A. R. M.; Dekker, C. *Nature* **1998**, *393*, 49.
(26) Collins, P. G.; Zettl, A.; Bando, H.; Thess, A.; Smalley, R. E. *Science* **1997**, *278*, 100.

NL048991S